Chapter

Tribological Study of the Friction between the Same Two Materials (RAD Steel)

D. Kaid Ameur

Abstract

These demands more and more severe of the organs of friction lead to operating temperatures of more and more high which result in particular a degradation of materials. This is reflected by decreases of performance that could jeopardize the safety (fall of the coefficient of friction) and penalize the economic balance (increase the wear). Our study highlights the interactions between the thermal, tribology, and physicochemistry and has been designed to respond to the following three objectives: (1) characterize at the macrolevel the phenomena of thermal localization and identify their influence on the coefficient of friction, (2) correlate to the local scale these phenomena to the physical mechanisms of friction, and (3) to identify the consequences of the degradation of the material with the temperature, based on the coefficient of friction and the physical mechanisms of friction.

Keywords: tribology, friction, materials, steel, degradation

1. Introduction

This study clearly showed the influence of the degradation of the material on the tribological behavior. However, the diversity of the elements in the presence complicates the interpretation of results.

Finally, the important role of the oxidation has also been highlighted in this study, by its contribution to the degradation of the material on the one hand, to the training of oxides present in the third body, on the other hand. This influence of oxidation could be investigated through the realization of tribological tests under a controlled atmosphere. As an exploratory measure, development on the triometer of an experimental device designed to deprive the contact of the oxygen in the ambient air has been undertaken in this spirit.

2. Proprieties

RAD (Aubert & Duval): A ball bearing steel, and as such previously only used by forgers, it is available in bar stock now (**Figure 1**). It is similar to 5160 (though it has around 1% carbon vs. 5160 ~ 0.60%), but holds an edge better. It is less tough than 5160. It is used often for hunting knives and other knives where the user is

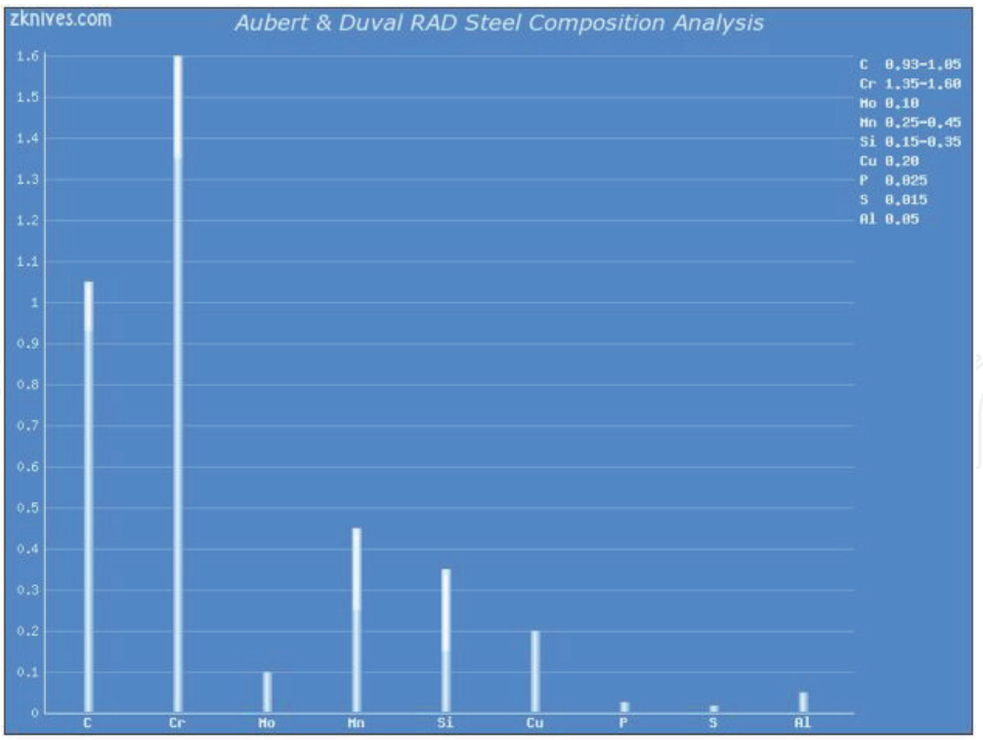

Figure 1.
RAD (Aubert & Duval) steel composition analysis.

willing to trade off a little of 5160's toughness for better wear resistance. However, with the continued improvement of 52,100 heat treat, this steel is starting to show up in larger knives and is showing excellent toughness. A modified 52,100 under the SR-101 name is being used by Jerry Busse in his Swamp Rat knives. The German equivalent 1.3505 has been discontinued [1].

It is used in precision ball bearings and many industrial applications. The balls made of this kind of material feature an excellent surface finish, considerable hardness, and a high load-carrying capacity, as well as excellent wear and deformation resistance. Chrome steel balls (**Figure 2**) are through hardened in order to achieve the maximum mechanical strength [2].

Diameters: 0.025–250 mm.

Precision grades: ISO 3290 G3–5–10–16–20–28–40–100–200–AFBMA G500/G1000.

Equivalent materials to international standards: AFN 100C6–B.S. EN 31–JIS G4805–SUJ2–ASTM 100C6.

Through hardness index:

Up to 12.7 mm HRC 62/66.

From 12.70 to 50.80 mm HRC 60/66.

From 50.8 to 70 mm HRC 59/65.

From 70 to 120 mm HRC 57/63.

Mechanical properties:

Critical tensile strength: 228 kgf/mm^2.

Compression strength: 207 kgf/mm^2.

Modulus or elasticity: 20,748 kgr/mm^2.

Specific weight: 7830 kgf/mm^2.

Chemical compositions, %:

C: 0.90–1.10; Si: 0.15–0.35; Mn: 0.25–0.45; P: 0.025–max; S: 0.025–max; Cr: 1.30–1.60.

Figure 2.
Chrome steel balls.

3. Characterization of the tribological behavior of the dry contact

3.1 Analysis of friction, μ, and μe

The friction coefficient is determined from the tangential force, Q*, measured during the test by a force sensor, and the normal force applied, P, measured by a sensor to gauge the constraints (**Figure 3**) [3].

The value of the coefficient of friction conventional said during each cycle is given by the following expression [4]:

$$\text{ì} = Q*/\text{P} \tag{1}$$

While the average value of the coefficient of mechanical friction during the entire test is expressed by the following expression [5]:

$$\overline{\mu} = \frac{1}{N_t}\sum_{i=1}^{N_t}\mu(i) \tag{2}$$

where N is the number of cycles (**Figure 4**).

$$\mu_e = \frac{E_d}{4*P*\delta_g} \tag{3}$$

where E_d is the dissipated energy in Joules, δ_g is the amplitude of slipping in micrometers, and P is the normal force applied in Newtons.

The average value of the energy coefficient of friction during the entire test is expressed by the following [4]:

$$\overline{\mu}_e = \frac{1}{N_t}\sum_{i=1}^{N_t}\mu_e(i) \tag{4}$$

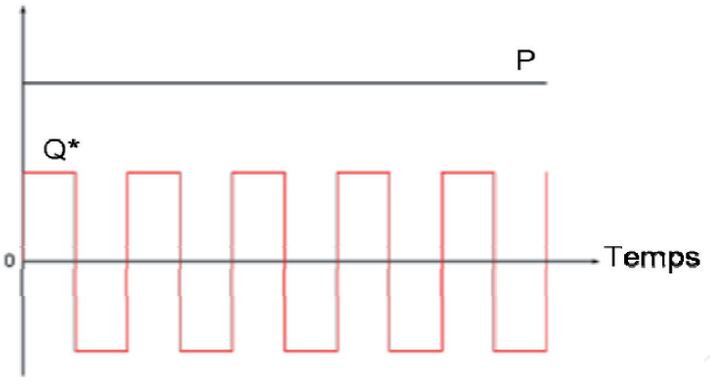

Figure 3.
Illustration of the evolution of the normal force and tangential force during the test (ideal situation of a rolling contact infinitely rigid) tangential as a function of time.

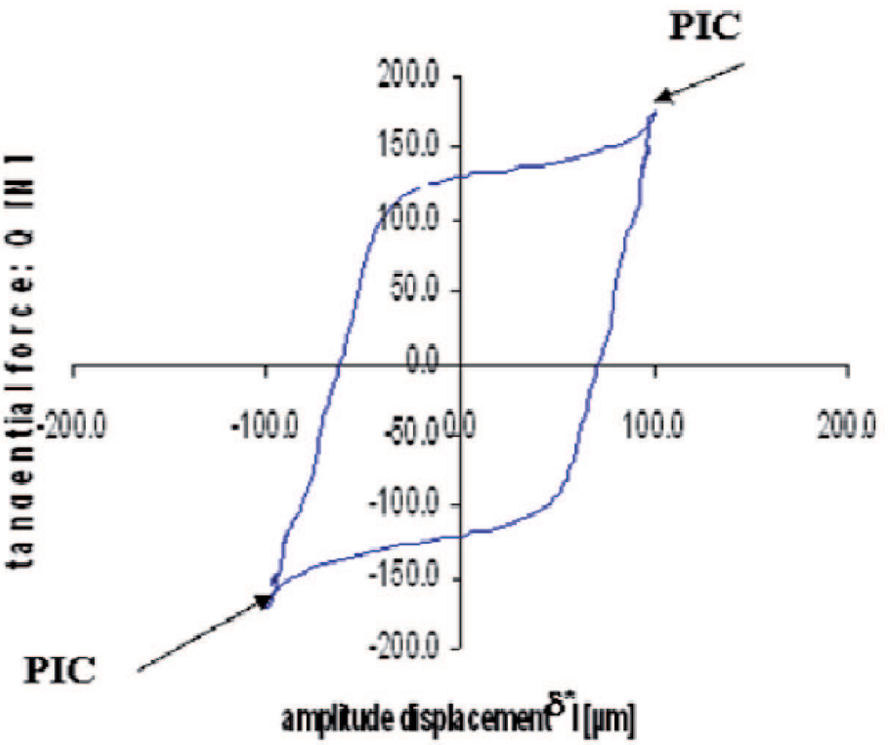

Figure 4.
Cycle of fretting during the test.

To study the evolution of the coefficient of friction during the test, we used a sphere contact/plan of steel 100Cr6 on the machine I, and the diameter of the SPHERE chosen is of 25.4 mm, and the movement is alternative straight with an amplitude of displacement of ±100 mm to a frequency of 10 Hz. A normal load of 86 N is applied during the test friction, which corresponds to a pressure of Hertzian contact maximum in the early test (without wear) of 1.1 GPa. The frequency of the movement and the frequency of the normal load are measured, recorded, and regulated during the test. The tangential force of contact is measured and recorded during the friction (**Figure 5**).

3.2 Evolution of the coefficient of friction

The evolution of the friction coefficient, μ, conventional and the energy coefficient, μe, in function of the cycles of fretting is presented in **Figure 6**. We

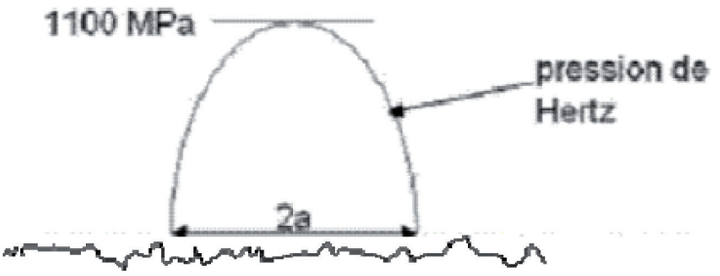

Figure 5.
A mapping of the initial contact sphere/plan for a load applied normal, 86 N (a is the radius of the contact terrestrial, we will appoint subsequently by a_H).

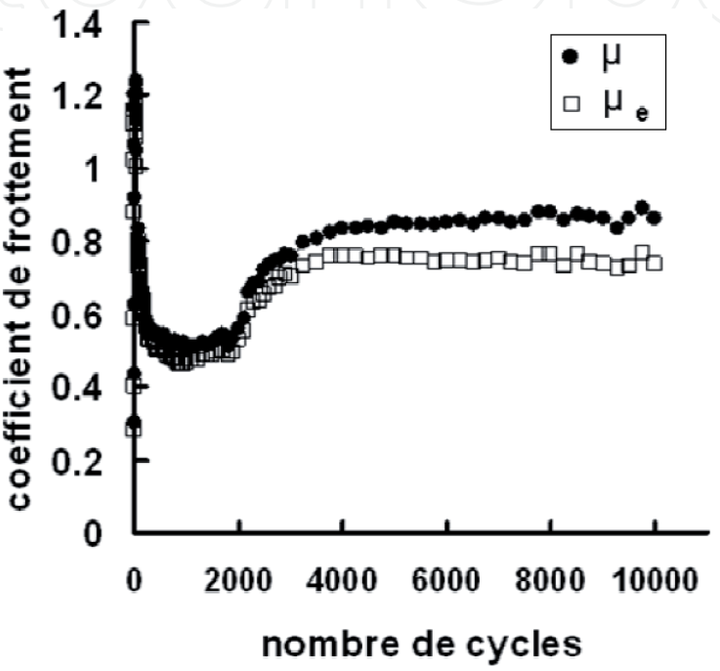

Figure 6.
Evolution of the coefficient of friction is conventional and of the energy coefficient. The friction in function of the number of cycles of fretting of the contact sphere/plan.

note that the evolution of μ and μe presents a similar evolution [6, 7]. The two curves are superimposed up to 2000 cycles, and while the contact stabilizes, we note a significant differentiation of μ and μe. The value of μ stabilizes around 0.85, while μe stabilizes at around 0.75. The values' averages over the whole of the test are, respectively, μ = 0.77, and μe = 0.71. Subsequently, it conducts tests that are interrupted following the evolution of the coefficient of friction (**Figure 7**, six conditions of the number of cycles of four cycles to 10,000 cycles) to appraise the structure of the traces of wear of the plan and of the sphere in function of the establishment of the contact. It still maintains the amplitude of slip, δg, and the amplitude of oscillation, δ*, as constant while all the tests are carried out.

The evolution of the coefficient of friction reveals three phases. During the first phase, we note an increase in the coefficient of friction up to a value of 1.2 (up to 20 cycles); then the second phase corresponds to a fall of up to 0.45 (up to 300 cycles); and then the third phase presents two parts: the first, an increase very progressive of the friction coefficient of 0.45–0.75 (of the 300th–3000th cycle). And finally, the second part of the third phase corresponds to a stabilization of the coefficient of friction around 0.85 (ranging from the 3000th–10,000th cycle).

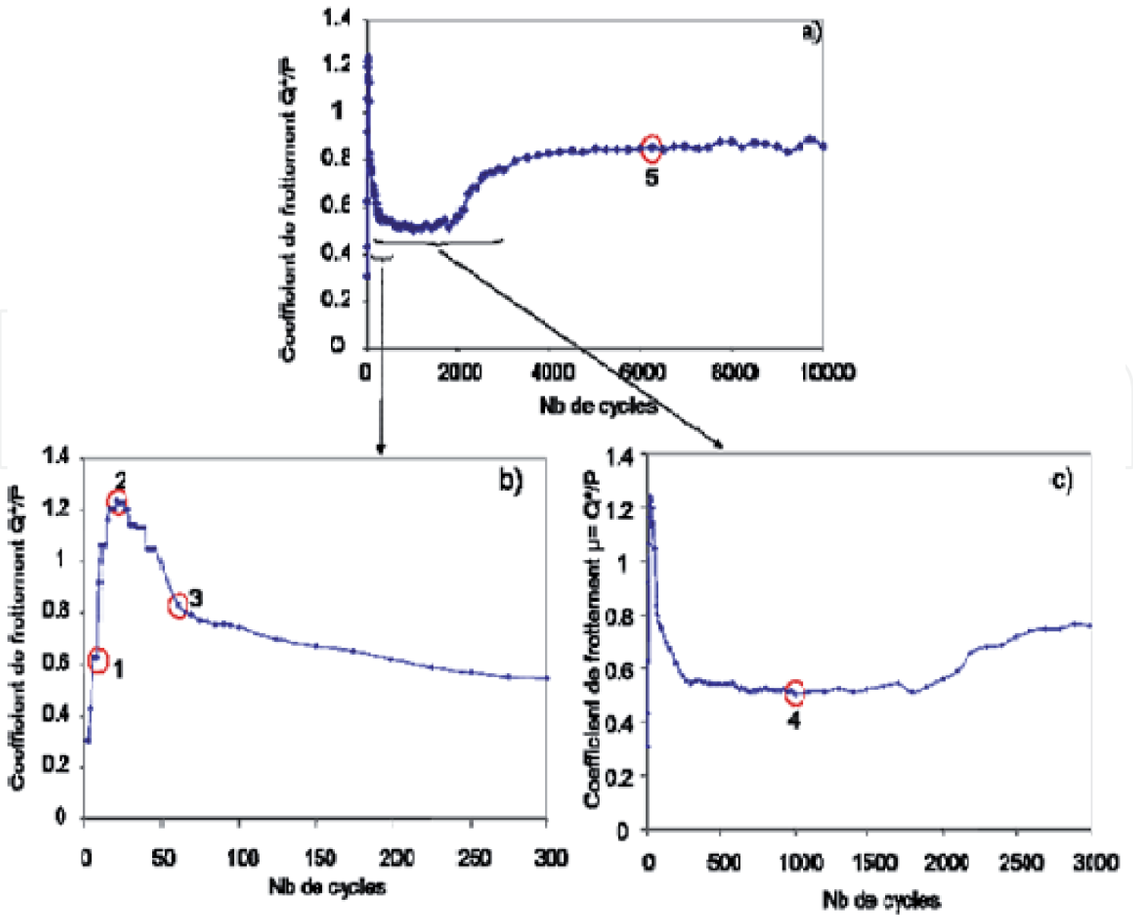

Figure 7.
Evolution of the coefficient of friction in function of the number of cycles for the torque 100C6 sphere/plan (F = 86 N, δ = 100 μm, F = 10 Hz, and R = 12.7 mm). (a) Test INTEGER, (b) zoom up to 300 cycles, and (c) zoom up to 3000 cycles, and the red circles indicate the tests interrupted for the expertise of traces of fretting.*

3.3. Analysis of the trace of wear

Several technics have been used to understand the evolution of the coefficient of friction. In function of the number of cycles: optical microscopy, the electronic microscopy to Sweep (SEM), as well as the EDX analysis [8, 9].

The observation of the traces of wear in the optical microscope after different durations of friction allows us to understand the evolution of the creation of debris and oxides in function of the time. The two surfaces, that of the sphere and that of the plan, are observed. The coloration of the trace of wear gives indications on the presence of oxides.

The SEM is used in order to achieve chemical analyses in the trace of wear and outside of the trace. These analyses confirm about the presence of oxides.

During the first phase, the increase, very brutal, of the coefficient of friction is associated with a contact metal/metal. We interrupt the test in the fourth cycle for observing the surface (**Figure 8**). We note that there is a large surface not worn to the inside of the contact and that we have a wear at the edge of the contact which is more important on the sphere on the plan.

The surface does not oxidize debris. In contrast the surfaces. The darkest shows transfers metal/metal, which explain the very strong increase in the coefficient of friction. Then interrupts our test to 20 cycles, and when the increase of the coefficient of friction reaches its maximum to observe the evolution of the trace of wear (**Figure 9**), we note the existence of a few debris at the edge of the contact, as shown in **Figure 9(c)**, where they are compacted, favoring the phenomena of accession at the edge of the contact, as shown in **Figure 9(d)**.

Analyses of EDX in the trace of wear have intended to assert or non-The presence of oxides in the trace of wear.

Figure 10(a) shows an image SEM of the trace of wear on a sample after 20 cycles of friction. An EDX analysis of the trace of wear (**Figure 10(b)**) shows the detectable elements as in **Table 1**.

Table 1 shows that there has been very little of oxides in the trace of wear to 20 cycles. **Figures 9** and **10** confirm a generalization of the metal-metal interactions after only 20 cycles, which allows us to explain the very high value of the coefficient of friction. In the second phase during the fall of the coefficient of friction, it stops

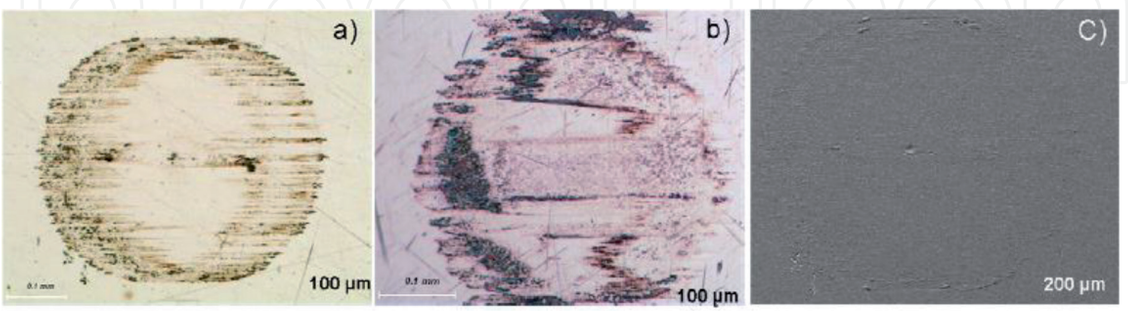

Figure 8.
Traces of wear on the samples to the fourth cycle. (a) Image under the microscope optics of the plan, (b) image in the optical microscope of the SPHERE, and (c) image to the SEM of the plan [10].

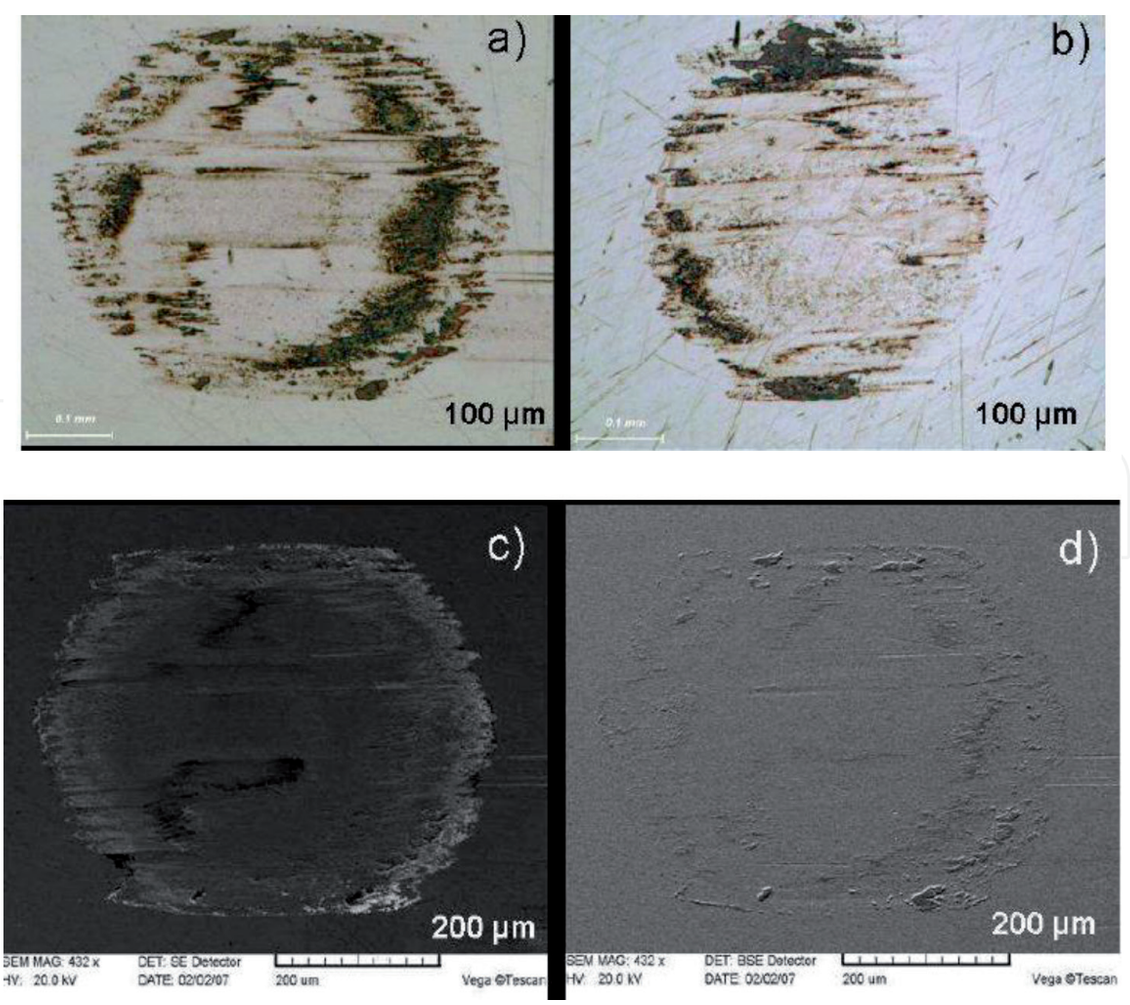

Figure 9.
Traces of wear on the samples in the twentieth cycle. (a) Image under the microscope optics of the plan, (b) image in the optical microscope of the SPHERE, and (c) and (d) image in the WPM in traces of wear [10].

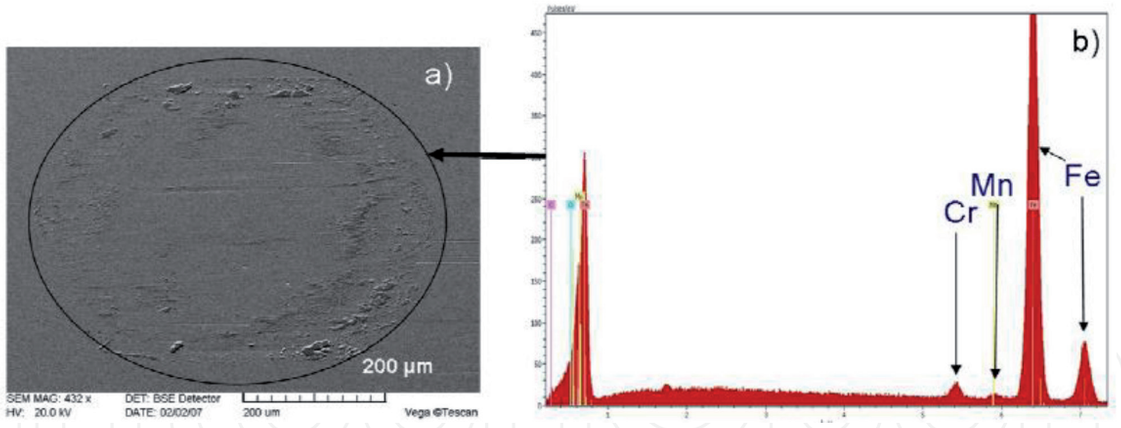

Figure 10.
Chemical analysis of the trace of wear on a sample after 20 cycles of friction. (a) Image SEM of the trace of wear and (b) EDX analysis of the trace.

Item	Atom (%)
Carbon	16.22
Oxygen	0.004
Chrome	1.76
Iron	82

Table 1.
Elements detected in the trace of wear to 20 cycles.

the test at the 60th cycle. The coefficient of friction is of the order of 0.8. **Figure 11** shows the different surfaces observed.

We note that there is a material removal to the inside of the contact (**Figure 11a**, **b**, and **d**). The fall of the coefficient of friction in the second phase is due to the presence of debris that are very oxidized (**Figure 11c**; the debris of white color observed using the WPM, which are ejected at the edge of the contact). After cleaning, it shows the existence of oxides on the worn surface, however, the EDX analysis shows results similar to those observed after 20 cycles with a few traces of oxygen (0.004%) on the surface worn. To locate these traces of oxides, it carries out analyses following a line called "Line Scan." These analyses are carried out line by line on the surface of the traces worn globally. One of these lines shows the presence of a few traces of oxide on the compacted materials at the edge of the trace of wear, as shown in **Figure 12**.

In conclusion, it could be deduced that after 60 cycles, of the first oxidized debris are trained and allow a partial reduction of the coefficient of friction. These debris are however few and are only little members in the interface (because they are easily eliminated). This allows you to explain that the coefficient of friction at this stage remains relatively high. Their accumulation in edge of contact suggests a change of load transfer and flotation a dela pressure on the edges of the contact. A fourth test is conducted and interrupted after 1000 cycles. This condition of solicitation corresponds to the coefficient of friction the lowest ($\mu = 0.5$). To interpret the tribological behavior, it is interesting to compare the optical observations and SEM (**Figure 13**) and the analysis of the surface of the contact (**Figure 14**).

Figure 13 shows that the material removed is distributed over the entire surface of the sphere and the plan [**Figure 13(a)–(c)**]. **Figure 13c** confirms the presence of a large quantity of oxides on the surface, before cleaning, and mainly distributed on the periphery of the contact. By contrast, after cleaning,

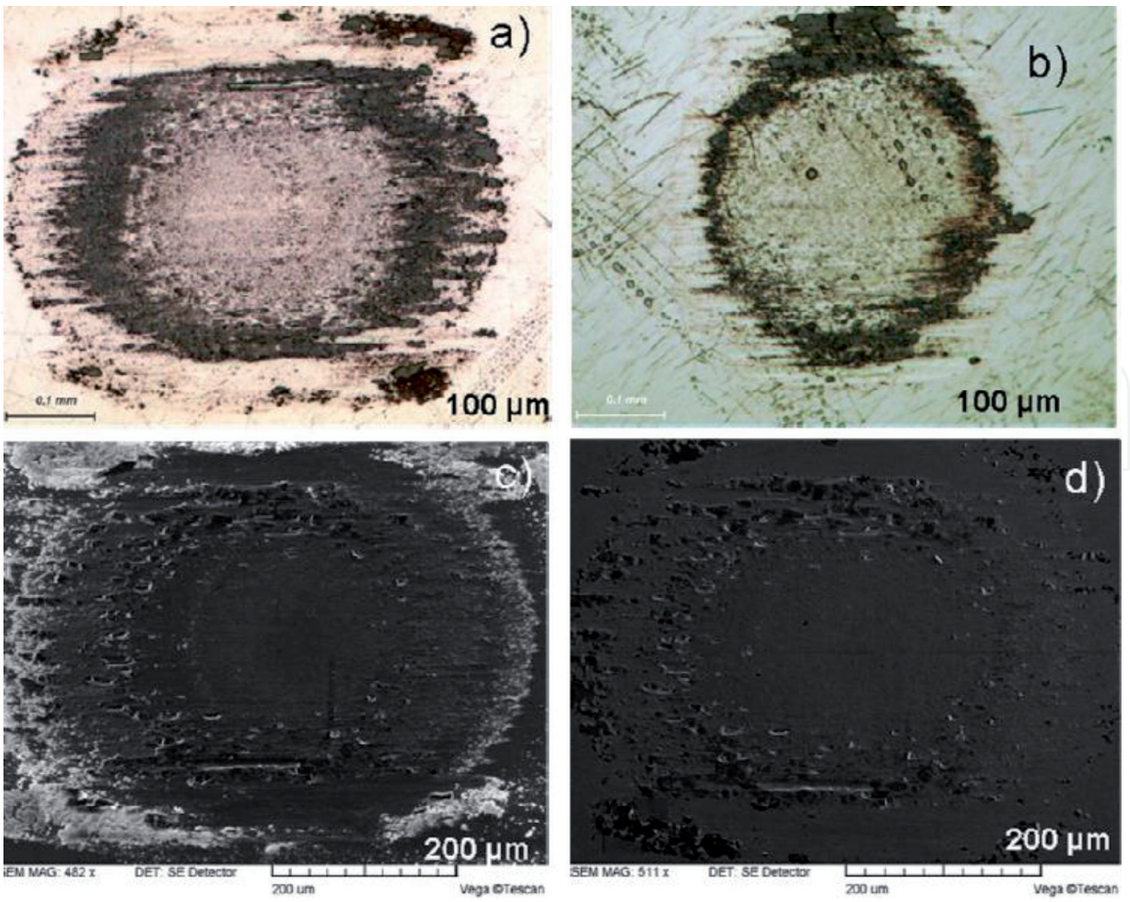

Figure 11.
Trace of wear after 60 cycles of friction. (a) Optical image of the plan, (b) image perspective of the SPHERE, (c) image in the WPM before cleaning, and (d) image to the SEM after cleaning [10].

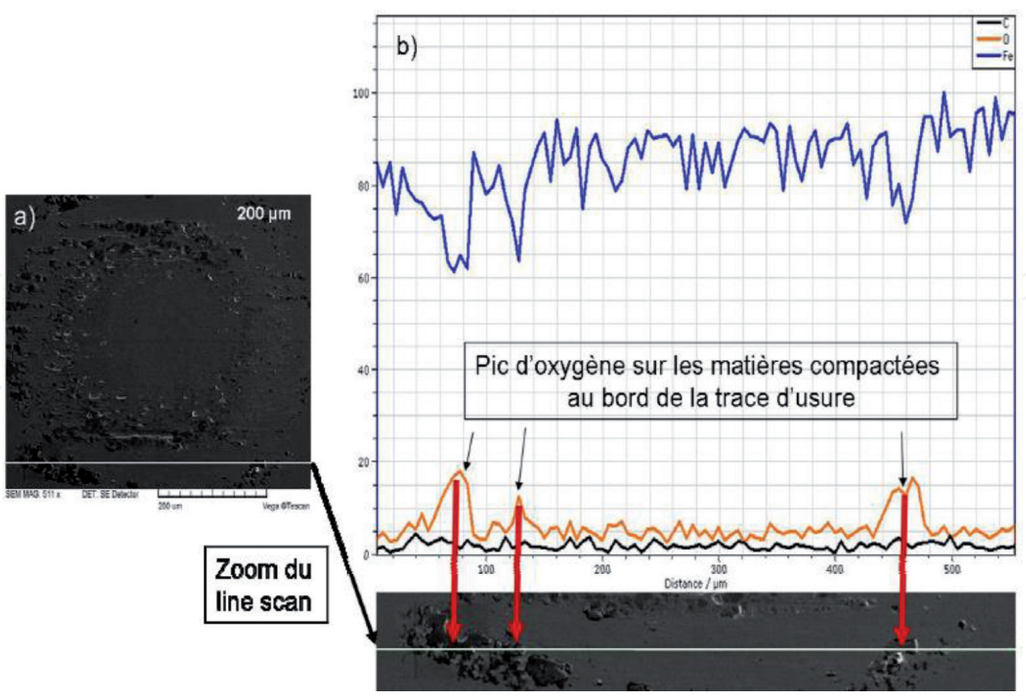

Figure 12.
Analysis of the line scan of the trace of wear on a sample after 60 cycles of friction. (a) Image SEM of a line scan of a plan and (b) zoom of the line scan with the results of EDX of this line scan.

the quantity of debris oxidized is much more low. The EDX analysis (**Figure 14**), however, confirms the presence of a large quantity of oxygen from the acceding debris in the interface.

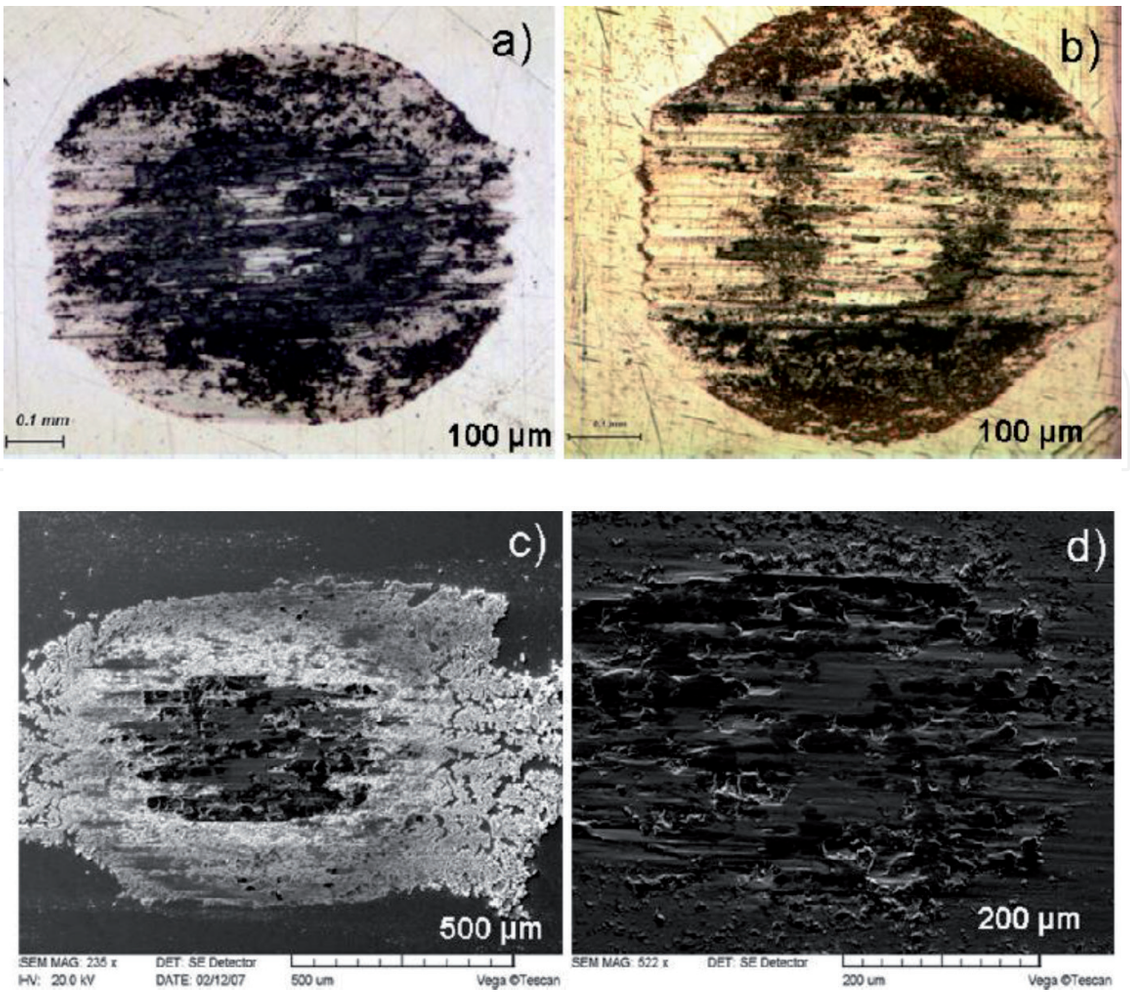

Figure 13.
Trace of wear on a sample after 1000 cycles of friction. (a) Image optics of the plan, (b) optical image of the SPHERE, (c) image to the SEM plan before cleaning, and (d) image to the SEM plan after cleaning [10].

Figure 14 also confirms the existence of oxidized debris on the sphere, especially at the edge of the contact. The concentration in oxides is confirmed by the semi-quantitative analysis (**Table 2**).

What we can remember is that the interface associated with the lowest coefficient of friction corresponds to a structure with a lot of debris oxidized very pulverulently because they are very easily eliminated (comparison of observations of SEM before and after cleaning); mainly located on the outer edges of the contact, this bed of debris very accommodating; and allows to obtain a coefficient of friction that is relatively low. The presence of debris more compacted and members indicates the activation of a process of "Mécano alloying" and the creation at the level of the first body of compacted debris more members. The fifth point analyzed corresponds to a test duration of 6000 cycles. It corresponds to the stabilized state, of contact with a value of the coefficient of friction of the order of 0.8, which is significantly greater than the point of intermediate 5.

Figure 15 illustrates the structure of the interface. It will be noted that these observations have been carried out after cleaning of surfaces.

One can conclude that a layer of compacted oxide is adherent and is distributed on the whole surface of the contact (**Figure 15d** and **e**). It confirms the very large quantity of oxides associated to acceding debris by the semiquantitative analysis of EDX (**Table 3**).

Figure 16 confirms that a similar pattern to that observed on the plan is activated on the sphere. In effect, even after cleaning of surfaces, there is a very large

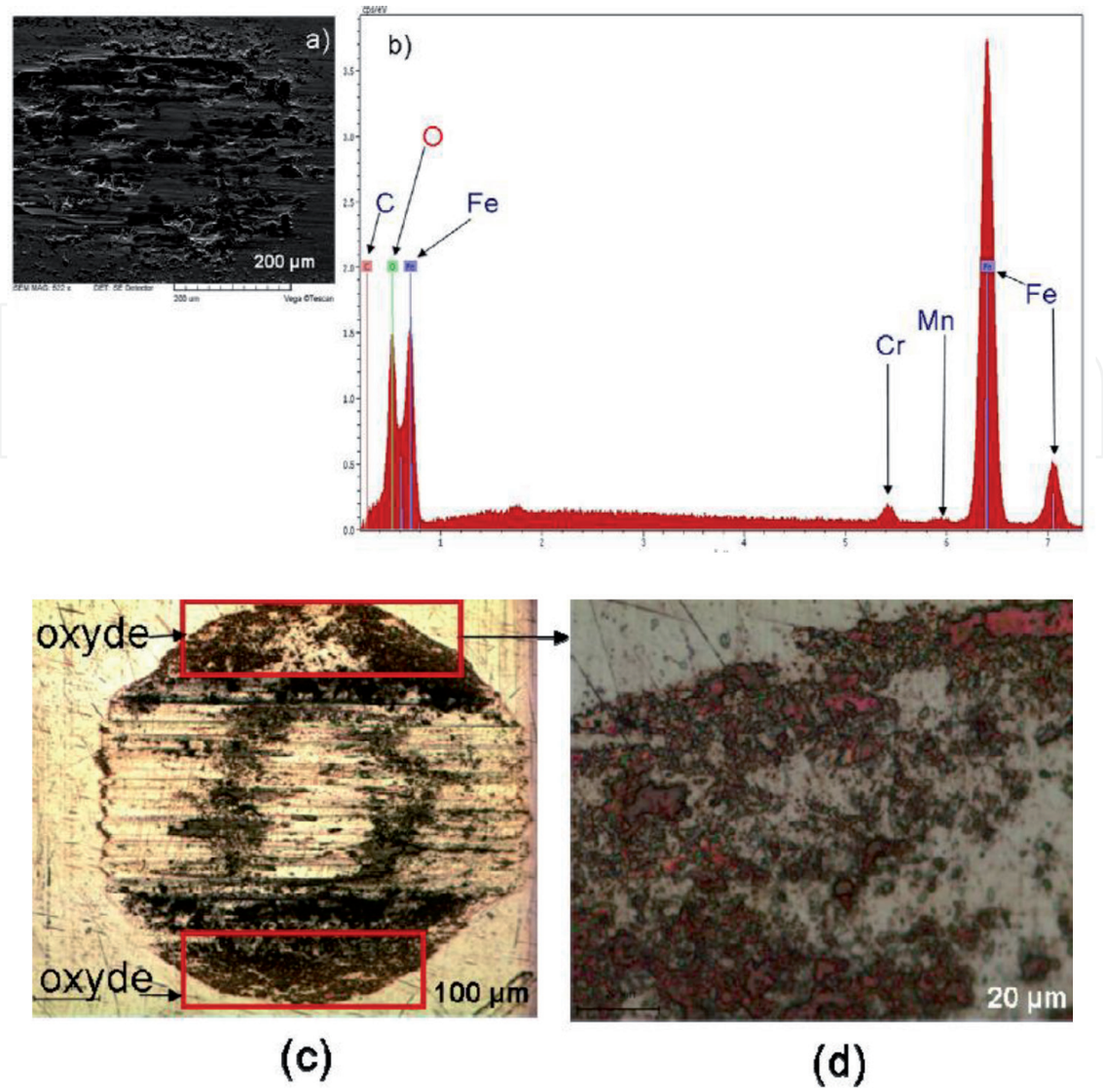

Figure 14.
Chemical analysis of the trace of wear on a sample of the plan and of the SPHERE after 1000 cycles of friction. (a) Image SEM of the trace of wear of the plan, (b) EDX analysis of the trace, (c) optical image of the SPHERE, and (d) zoom of the oxidized portion of the SPHERE [10].

Item	Atom (%)
Carbon	16.9
Oxygen	15.6
Chrome	1.5
Iron	65.8

Table 2.
Elements detected in the trace of wear to 1000 cycles.

quantity of oxides acceding compacted on the surface. In conclusion, it is shown that the process already observed after 1000 cycles of compaction of the third body is becoming widespread. The interface thus evolves to a structure, little member of a third cohesionless body toward a third body compacted, very adhesive.

This evolution of the rheology of the third body, which gives rise to a 3rd Corps member and less complacent than that the bed of cohesionless debris, may explain the increase in the friction coefficient of the second minimum at $\mu = 0.5$, up to the bearing stabilized at $\mu = 0.8$.

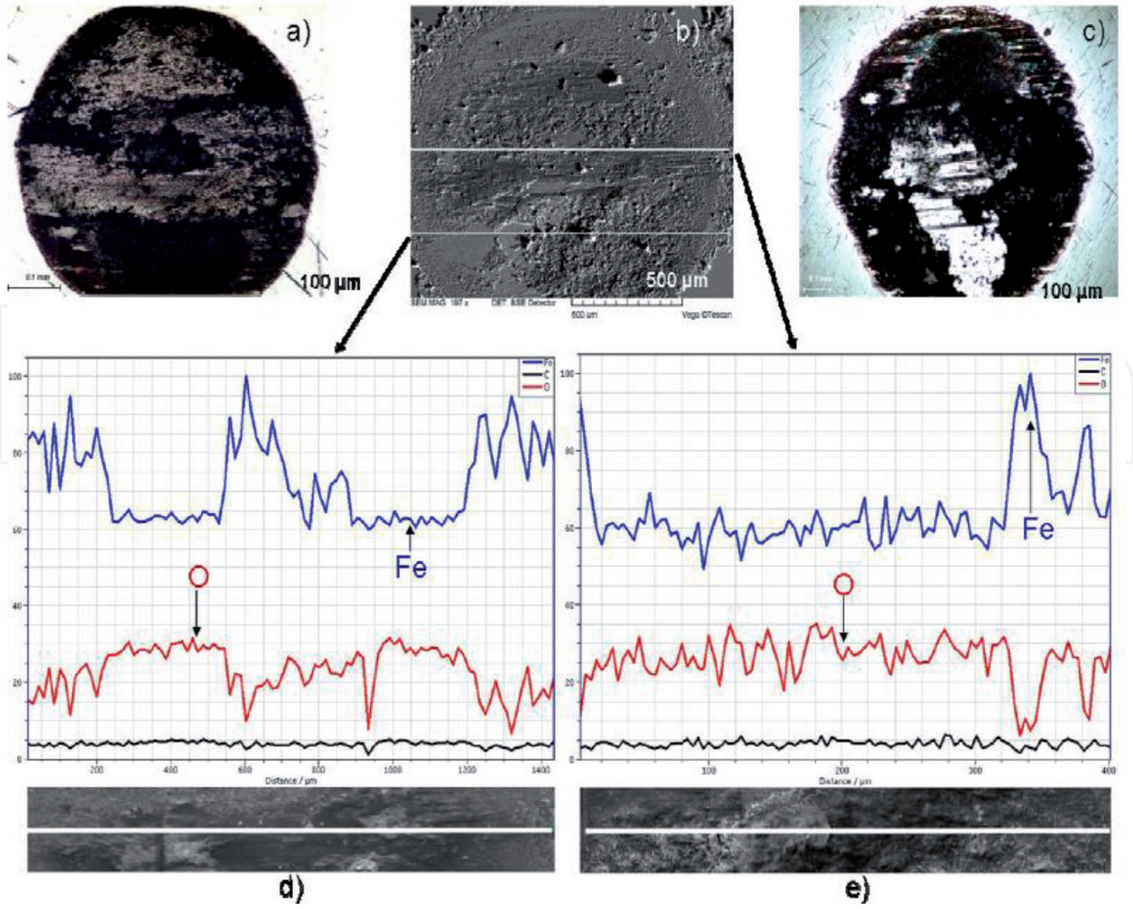

Figure 15.
Traces of wear and chemical analysis of traces of wear on a sample after 6000 cycles of friction. (a) Optical image of the plan, (b) image SEM of the plan, (c) image perspective of the SPHERE, (d) zoom of analysis scan line at the edge of the contact, and (e) zoom of analysis line scan in the middle of the trace of wear.

Item	Atom (%)
Carbon	10.6
Oxugéne	28.3
Chrome	1.4
Iron	59.6

Table 3.
Elements detected in the trace of wear to 6000 cycles.

4. Discussion

The coupled analysis between the evolution of the coefficient of friction and the structure of the interface allows us to establish the tribological scenario next (**Figure 17**).

The very low coefficient of friction observed at the beginning of the test corresponds to an interface involving the native oxides (A). Very quickly, the layer of oxides is eliminated and there is a sharp increase in the coefficient of friction related to activation of interactions metal/metal (B). The interactions metal/metal generalize and generate a maximum shear in the interface (C). The very high stresses generated in the interface lead to formation of debris that oxidize. The interface is more accommodative and the coefficient of friction tends to decrease (D).

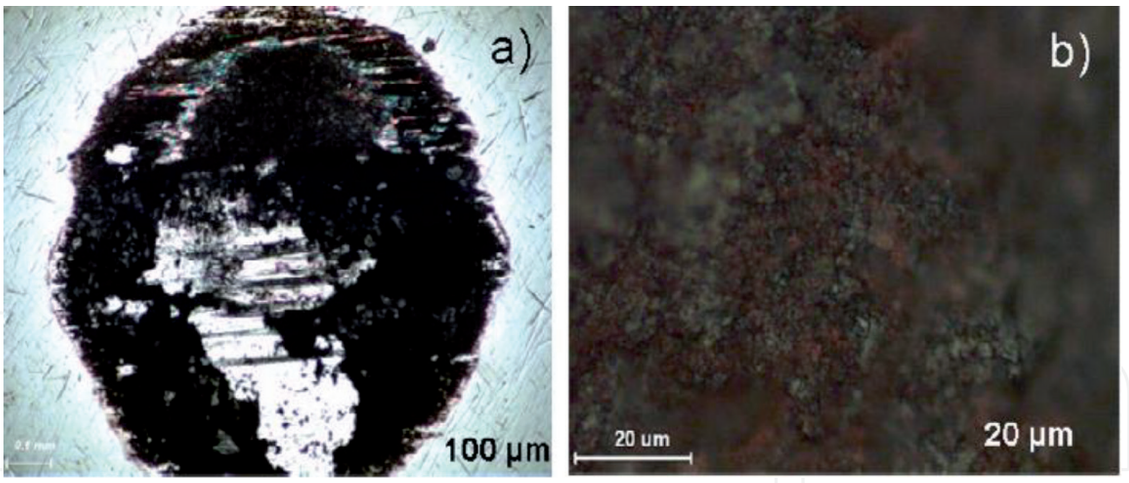

Figure 16.
Traces of wear on the samples after 6000 cycles. (a) Image under the microscope perspective of the SPHERE and (b) zoom of the trace of wear [10].

The training of cohesionless debris generalizes and finally écrante interactions metal/metal. Fully accommodated by a third body, very cohesionless, divided on the periphery of the contact, the interface then presents a second minimum of its coefficient of friction (E).

Under the mechanical action of the loading of fretting, the bed of debris then tends to be compressed. It becomes more adherent and generalizes on the whole of the interface. Less complacent than the bed cohesionless debris (Step e), it presents a coefficient of friction higher (F) of the order of ($\mu = 0.8$). If the evolution between the steps a and e is classically described in the literature, the transition between E and F that we have analyzed clearly shows the influence of rheology in the interface.

Having analyzed the response of the friction coefficient of the dry contact, we will discuss in the next chapter, the response by report to the wear.

5. Conclusion

The objective of this study was to analyze the behavior in fretting of the steel contact. The expertise of the industrial systems in fact appear of slip conditions, total inducing large amplitudes of slip, thus favoring the degradation of the assembly by wear. There is a real need in the industry to have predictive methods about the mechanisms of wear, to limit maintenance inspections while ensuring an optimum level of security.

For the first time, the coupled analysis of the evolution of the coefficient of friction and the structure of the interface allows us to divide the evolution of the coefficient of friction into six phases, appointing A, B, C, D, E, and F and describing the scenario of the evolution of the interface as well as the role of the debris and oxides in the contact.

The elimination of the layer of native oxides (A and B) generates the interactions of metal/metal, which promotes a maximum shear in the interface (C). The training of debris that oxidize tends to decrease the coefficient of friction (D and E). Under the mechanical action of the loading of fretting, the bed of debris then tends to be compact and becomes more adherent, and it generalizes on the whole of the interface. This third compacted body, less complacent than the bed of the cohesionless debris, may cause an elevation of the coefficient of friction (F).

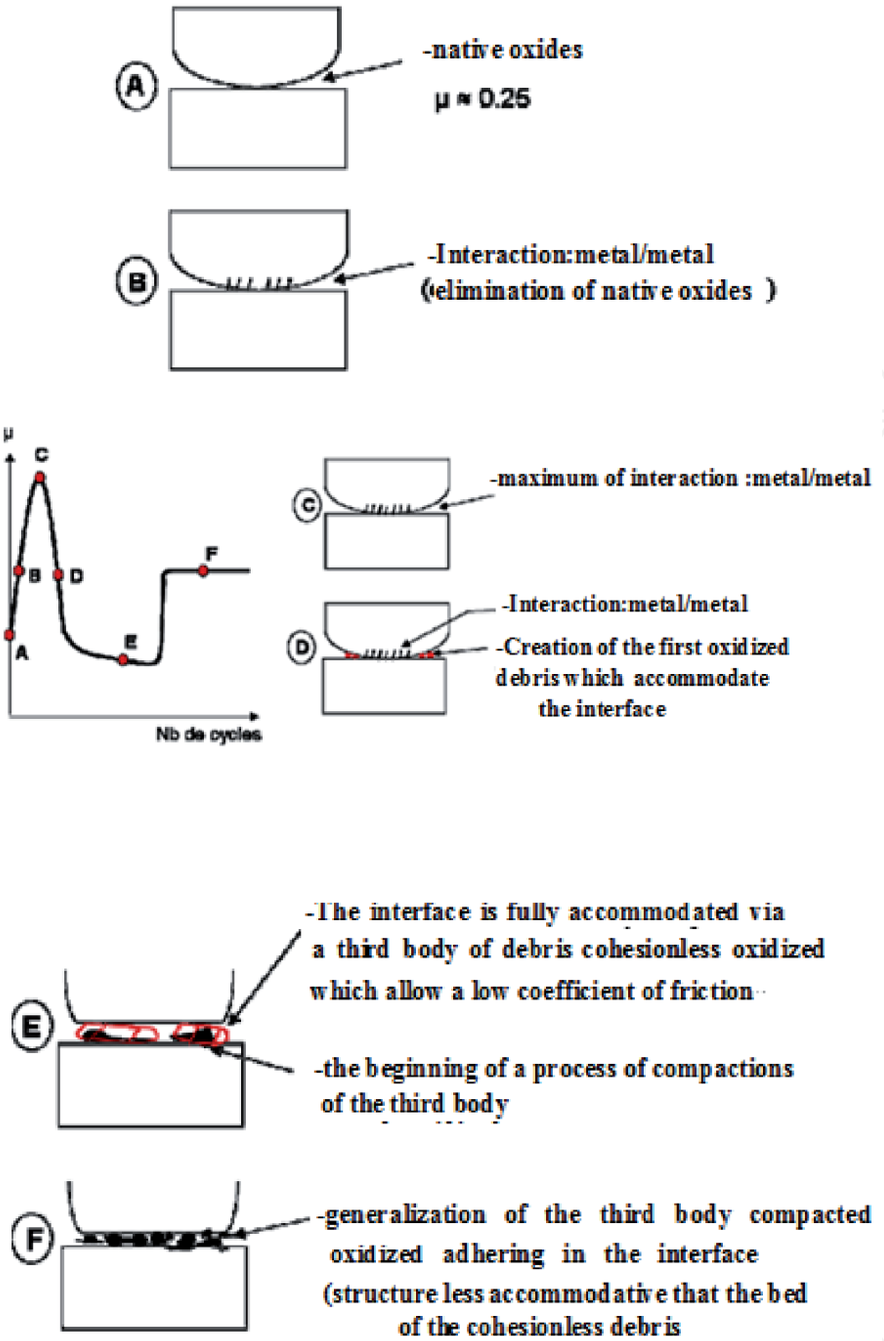

Figure 17.
Illustration of the scenario describing the evolution of the interface and that associated to the coefficient of friction.

By that result, we sought to quantify the kinetics of wear. The successive damage the contact has been formalized through the approaches of Archard and the dissipated energy. The evolution of the coefficient of friction for different sizes of contact shows that the more the contact, the lower the coefficient of friction of the stabilized phase (F). It can assume that larger contact facilitates the trapping of oxidized debris in the contact.

The interface will be more accommodative and will induce a coefficient of friction that is more low. By elsewhere, a greater amount of energy will be dissipated in the third body and not to the level of the first body for the creation of new debris so that the kinetics of wear will also be lower for the great contacts.

IntechOpen

Author details

D. Kaid Ameur
Laboratoire de Génie Industriel et du Développement Durable (LGIDD), Centre Universitaire de Relizane, Bormadia, L'Algérie

*Address all correspondence to: djilalikaidameur@gmail.com

References

[1] (Aubert § Duval RAD Steel)

[2] CHROME_STEEL_BALLS_ AISI_52100_UNI100C6-htm_s13lccgu-NormeAFNOR Française

[3] Berthier Y. Background on friction and wear. In: Lemaître Handbook of Materials Behavior Models.. Section 8.2. Academic Press; 2001. pp .676-699

[4] Bettge D, Starcevic J. Topographic properties of the contact zones of wear surfaces in disc-brakes. Wear. 2003;**254**:195-202

[5] Bulthé A-L, François M, Desplanques Y, Degallaix G. Comportement d'un couple disque-patin sous sollicitations de freinage et observations in situ du 3ème corps. In: 17ème Congrès Français de Mécanique Troyes. 2005

[6] Bulthé A-L, Desplanques Y, Degallaix G, Berthier Y. Mechanical and chemical investigation of the temperature influence on the tribological mechanisms occurring in OMC/cast iron friction contact. In: 12th Nordic Symposium of Tribology, NordTrib 2006 Helsingor (Danemark). 2006

[7] Cho MH, Kim SJ, Kim D, Jang H. Effect of ingredients on tribological characteristics of a brake lining: An experimental case study. Wear. 2005;**258**:1682-1687

[8] Copin R. Etude du comportement tribologique de couples de matériaux industriels sur tribomètre reproduisant les conditions de freinage ferroviaire [thèse]. Université des Sciences et Technologie de Lille; 2000

[9] Desplanques Y, Roussette O, Degallaix G, Copin R, Berthier Y. Analysis of tribological behaviour of pad-disc contact in railway braking. Part 1: Laboratory test development, compromises between actual and simulated tribological triplets. Wear. 2006. In press

[10] Merhej R. Matériaux [PhD thesis]. France: Ecole Centrale de Lyon; 2008